Wavepackets and inelastic tunnelling

1993 J. Phys.: Condens. Matter 5 5141

(http://iopscience.iop.org/0953-8984/5/29/010)

J. Phys.: Condens. Matter 5 (1993) 5141–5158. Printed in the UK

Wavepackets and inelastic tunnelling

A Bringer†, J Harris† and J W Gadzuk‡

† Institut für Festkörperforschung, Forschungszentrum Jülich GmbH, D-5170 Jülich, Federal Republic of Germany

‡ National Institute of Standards and Technology, Gaithersburg, MD 20899, USA

Received 15 March 1993

Abstract. Using real-time numerical propagation techniques, we consider the tunnelling of electron wavepackets through potential barriers that possess internal dynamics. The models considered allow the study of the influence of localized surface vibrational modes on the tunnel current observed in scanning tunnelling microscopy. Non-resonant and resonant processes are considered. In the former case, we focus on the behaviour of the total tunnel current when the energy sweeps through an inelastic threshold. In the resonant case, we make contact with analytic theory and consider in detail, using a two-channel Breit–Wigner model, the physics underlying the resonant process, the physical origin of sum-rules obeyed by the tunnelling characteristic, and the conditions under which simple analytic theoretical results can be applied in general.

1. Introduction

The study of tunnelling phenomena in solid state structures such as quantum wells [1] and scanning tunnelling microscopes (STM) [2] is currently active, both because of intrinsic scientific interest as well as possible short-term practical payoffs. One of the characteristics of the quantum well that gives rise to some of its intriguing tunnelling properties is the quasi-discrete nature of its eigenvalue spectrum. If the Fermi level of the tunnel structure playing the role of emitter or cathode is tuned to coincide with the energy of one of the quantum well's quasi-bound states, the electron transmission function undergoes resonant enhancement. Many years ago, this phenomenon of resonance tunnelling, as manifest in field emission energy distributions, provided the first experimental spectroscopic probe of the electronic structure of adsorbed atoms, based on a one-electron process [3]. In that particular case, the 'quantum well' was in fact the potential well of the single adsorbed atom or molecule, similar to the present view of tunnelling in an STM [2,4,5]. More commonly, quantum wells are associated with so-called nanostructures which have been fabricated using molecular beam epitaxy. Although quantum well states have been observed in systems as thin as a monolayer [6], the characteristic dimension of the various layers in sandwich configurations is typically of the order of tens of angstroms. This influences only the energy scale, however, and the nature and properties of resonant tunnelling are basically the same in nanostructure and STM contexts.

Inelastic processes in tunnelling are often discussed in terms of tunnelling times [7], particularly as embodied in a model due to Büttiker and Landauer [8] within which the inelasticity is due to an externally imposed modulation of a barrier or well property [8–11]. More generally, recent study [9, 10] has focused on the situation where the inelasticity is due to optical phonons, intramolecular vibrational modes, or some other boson excitations

0953-8984/93/295141+18$07.50

localized within the well [12–14], and has been formulated in terms of the useful model Hamiltonian [15]

$$H = H_{el} + H_{ph} + H_{int} \tag{1}$$

where

$$H_{el} = \epsilon_a c^\dagger c + \sum_{\kappa,\alpha} \epsilon_{\kappa,\alpha} c^\dagger_{\kappa,\alpha} c_{\kappa,\alpha} + \sum_{\kappa,\alpha} V_{\kappa\alpha,a}(c^\dagger_{\kappa,\alpha} c + c^\dagger c_{\kappa,\alpha})$$

$$H_{ph} = \hbar\omega_0 b^\dagger b \qquad H_{int} = \lambda_0 c^\dagger c(b^\dagger + b).$$

This describes a discrete electronic state localized in the quantum well (eigenvalue ϵ_a, fermion operators $c^\dagger$, c) coupled via matrix elements $V_{\kappa\alpha,a}$ to a number of electronic continua specified by α, with eigenvalues $\epsilon_{\kappa\alpha}$ and operators $c^\dagger_{\kappa,\alpha}$, $c_{\kappa,\alpha}$. This electronic system interacts with a dispersionless boson field described by a harmonic oscillator Hamiltonian, with the oscillator linearly displaced when the electronic quantum well state is occupied. The tunnel junction shown in figure 1 is conveniently characterized by this Hamiltonian with the sums on α restricted to two terms, in which $\alpha = l(r)$ refers to the continuum of electron band states in the left (right) electrodes. With the electrodes biased by $\Delta\mu$ as indicated in figure 1, the total amount of energy left in the vibrational system is balanced by the energy loss of the electron which has tunneled, which in turn has an upper bound equal to $\Delta\mu$.

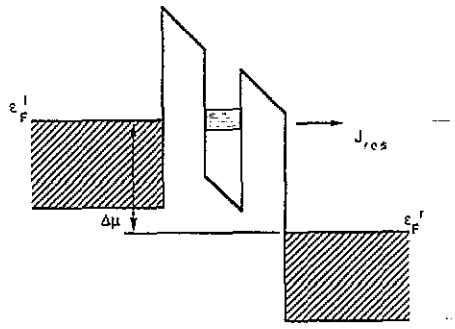

Figure 1. Sketch of a tunnel junction linking left and right metal electrodes with Fermi levels $\epsilon_F^{l,r}$ and possessing a quantum well in the interstitial region.

Although the model specified by (1) has been used in many different physical contexts over the past several years [15–17], mathematical simplifications are required to achieve an exact analytical solution. In the limiting case in which $\lambda_0 = 0$, the occupation probability of the resonance after initial creation at time $t = 0$, decays exponentially as $n_a(t) = \langle c^\dagger(t)c(t)\rangle = e^{-\Gamma t/\hbar}$ and the local density of states associated with the quantum well is a Lorentzian†. The width is expressed as $\Gamma = \sum_\alpha \Gamma_\alpha$, where $\Gamma_\alpha = 2\pi \mid V_{\kappa\alpha,a} \mid^2 \varrho_\alpha(\epsilon_a)$ with ϱ_α the density of states of the αth continuum at energy ϵ_a and $V_{\kappa\alpha,a}$ the constant hopping/tunnelling matrix element between the well and continuum/conduction band state.

When $\lambda_0 \neq 0$, the simple electron–phonon interaction in (1) amounts to a linearly displaced forced harmonic oscillator model [18], within which the time dependence of

† The exponential decay could occur even if $\lambda_0 \neq 0$, but the resulting local density of states would then be more complicated than the simple Lorentzian. This effect is always present when the decay is into a bounded continuum.

the force is related to the time dependence of the resonance occupation. For the single-level well, this occupation is at any given instant either zero or one, although the time-averaged occupation is fractional. The coherent fluctuations in the occupation result in sudden switchings on and off of H_{int}, which takes on values of either 0 or $\lambda_0(b + b^\dagger)$, but with no intermediate values as this would, in effect, require some internal degrees of freedom within the localized state† [20]. For a process involving a single sudden switch from the ground state of H_{ph} to $H_{\text{ph}}+H_{\text{int}}$ (or vice versa), the final oscillator state distribution is Poisson, with the probability of the nth state excitation given by $P_n = \exp(-\beta)(\beta^n/n!)$ where $\beta = (\lambda_0/\hbar\omega_0)^2$. For time evolution involving multiple switches, as in resonance tunnelling, the final distribution of excited states is more complicated but is still basically a variant of a product of Poisson distributions, one for each switch on or off of H_{int} augmented with interference effects‡.

The algebraic structure of the final result for a process governed by the Hamiltonian in (1) usually has the familiar form of a Poisson- or Gaussian-like expression, either convoluted with a Lorentzian or averaged over time with an exponential weighting factor [15–17]. This has been discussed explicitly with respect to inelastic resonant tunnelling through quantum wells [13, 17]. With the limitations implicit in (1), plus the consequences of the additional 'technical approximations' needed to obtain neat analytic solutions, it is legitimate to wonder what inelastic resonant tunnelling really 'looks' like [22], and whether the actualities of the process survived the modelling, simplifications and limiting case procedures that are necessary to set up explicitly soluble scattering state theories [13].

In order to address these issues, we have initiated quantum mechanical wavepacket simulations designed to model inelastic electron tunnelling through quantum well structures. The advantage of a wavepacket formulation is that, aside from numerical errors arising from the time propagation, scattering and reaction probabilities are given exactly whatever the coupling strength and the complexity of the coupling. A considerable body of expertise with regard to wavepacket dynamics has been built up in recent years, notably in connection with chemical physics and nuclear, rather than electron, motion [23, 24]. Fast Fourier transform (FFT) techniques for time-evolving wavefunctions projected onto a grid allow real-time study of multi-dimensional quantum systems. In the present study, we have adapted procedures developed previously in connection with reactive scattering [24] and with charge-transfer behaviour during ion–surface collisions [25] to the inelastic resonant tunnelling of electrons. Jauho and Jonson have considered a related problem, but on the assumption that the exchange of energy between electron and the degree of freedom responsible for the inelasticity does not influence the motion of this degree of freedom, i.e. they considered the motion of a one-dimensional wavepacket subject to a time-modulated potential well [10, 11]. This may be a valid approximation in non-resonant inelastic tunnelling, but is questionable in the resonant case. Although numerical limitations place some restrictions on the types of problems which can be treated sensibly via real-time wavepacket propagation (as will be discussed later), these are of a fundamentally different nature than the constraints required for the solution of (1). The methods are therefore complementary rather than competitive. We restrict ourselves here to simple model systems tailored to structures with STM-like dimensions [4], for which the wavepacket method is best suited.

† Parenthetically we note that this aspect of the simple displaced oscillator model could be inadequate for describing many modern ultrafast laser experiments, where the decay of an initially prepared state is followed as a 'function' of the 'preparation' dynamics. See, for example, [19].

‡ As a special example, if H_{int} is switched on and off at $t = 0, \tau_R$, then the distribution is still Poisson, but with the parameter $\beta(\tau_R) = 2\beta[1 - \cos(\omega_0\tau_R)]$. See [21].

The remainder of the paper is organized as follows. The wavepacket method and technical details of the calculations are presented in section 2 along with visual material illustrating how the packets behave in the non-resonant and resonant cases. In section 3 we consider specifically non-resonant inelastic tunnelling, focusing in particular on the question of unitarity and its connection with threshold behaviour. Inelastic resonant tunnelling is treated in section 4. Here the focus is on the structure in the tunnelling characteristic induced by the oscillator coupling. Results obtained with the wavepacket method are compared with the analytic formula derived by Wingreen and co-workers [13] on the basis of the Hamiltonian in (1). Excellent agreement is found. Also, some simple sum-rules obeyed by the analytic formula are found to be obeyed approximately by the numerical results. The physics underlying this comparison, and the physical origin of the sum rules is discussed in detail with the aid of a two-channel Breit–Wigner model. Finally, in section 5, we summarize and conclude.

2. Model description and technical details

The model used to study inelastic tunnelling is specified by the Hamiltonian

$$\hat{H} = -\frac{\hbar^2}{2m_e}\frac{\partial^2}{\partial X^2} + V_t(X) + \tfrac{1}{2}\hbar\omega(P_o^2 + Y^2) + V_c(X, Y) \tag{2}$$

comprising sequentially the electron kinetic energy, a stiff tunnelling barrier, a free oscillator Hamiltonian and an electron–oscillator coupling. The momentum and position operators of the oscillator, P_o, Y, are chosen to be dimensionless so the free oscillator is completely specified by its vibrational energy $\epsilon_{osc} \equiv \hbar\omega$; X is the position operator of the electron and the equivalent operator for the oscillator in the same units is $y = \alpha Y$, where $\alpha \equiv [\hbar^2/(M_{osc}\kappa)]^{1/4}$, with M_{osc}, κ the mass and force constant of the oscillator. The stiff tunnelling barrier comprises two contributions:

$$V_t(X) = V_0(X) + V_{res}(X) \tag{3}$$

where

$$V_0(X) \equiv \frac{V_0(1 + e^{-\beta X_c}) + V_R\Theta(X)e^{-\beta X_c}(e^{\beta X} - 1)}{1 + e^{\beta(|X| - X_c)}} \tag{4}$$

is a tunnel barrier between $-X_c < X < X_c$ with wall thickness β^{-1} and heights when approached from $-X, +X$ of $V_0, V_0 - V_R$, respectively, and

$$V_{res}(X) = -V_{res}\exp(-\gamma X^2) \tag{5}$$

is a resonance contribution in the form of an inverted Gaussian centred at the origin, $X = 0$. The electron–oscillator interaction is localized within the barrier and is assumed linear in the oscillator displacement. Specifically, the coupling is taken to be

$$V_c(X, Y) = -V_c Y\exp(-\gamma X^2) \tag{6}$$

where V_c measures the overall coupling strength. The tunnelling particle was taken to have the electron mass, $m_e = 1$, and the barrier parameters $V_0 = 10\,\text{eV}$, $\beta = 4\,\text{au}$, $\gamma = 1\,\text{au}$ were kept fixed in all cases.

For the non-resonant case, $V_{res} = 0$, a relatively thin barrier ($X_c = 2$ au) was used so the tunnel probabilities are large enough to be calculated easily using a wavepacket method. This is not a difficulty of principle, but it is much easier to ensure that numerical errors are eliminated if the tunnelling probabilities are not too small. The barrier was made asymmetric with $V_R = 4$ eV so that threshold behaviour in the final state could be studied easily. A sketch of the stiff barrier is shown in figure 2(*a*). Roughly, this may be regarded as modelling a weak-link metal–metal contact. The common 'Fermi level' (i.e. the lowest energy at which tunnelling into the right metal becomes possible) is at -6 eV with respect to vacuum and the bandwidth of the metal on the left is 4 eV. The tunnelling process envisaged involves a 'hot electron' (excited, for example, by a sub-picosecond laser pulse) incident from the left metal and traversing the barrier, where it couples via short-range forces to a local vibrational mode (due to a trapped molecule, for example).

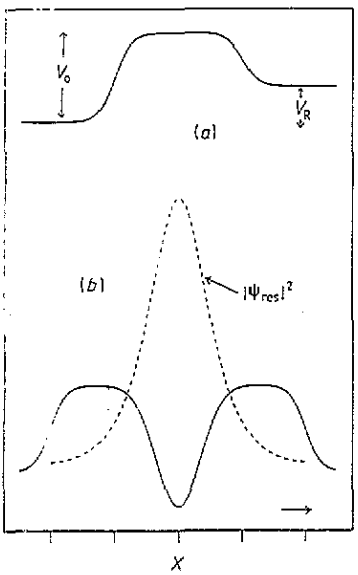

Figure 2. (*a*) Static barrier for non-resonant tunnelling. (*b*) Static barrier for resonant tunnelling with a sketch of the probability density of the resonant state. Potential parameters as given in the text. The coupling to the oscillator is localized within the barriers with a maximum at the barrier centres.

In the resonant case a symmetric barrier ($V_R = 0$) was used that was wider ($X_c = 4$ au) to accommodate the resonance region. The strength of the resonance potential was taken to be $V_{res} = 14$ eV. The stiff potential $V_t(X)$ in (3) then displays an elastic scattering resonance at 4.92 eV. A sketch of the potential and the stationary wavefunction at resonance is shown in figure 2(*b*). This can be regarded as simulating a similar situation to the above, but with the coupling to the inelastic degree of freedom enhanced dramatically because of the long 'delay time' of the electron within the barrier when the resonance condition is close to being fulfilled. The interplay is sufficiently strong so as to alter the resonance structure of the barrier qualitatively.

The tunnelling behaviour of these barriers was explored using wavepacket propagation. An incident free packet localized about $X = -X_0$ and with zero weight in the barrier region $X \sim 0$ was propagated using the split operator method of Feit and co-workers [23], i.e. time translation of the wavepacket is performed according to

$$\exp(-i\hat{H}\tau) = \exp\left(-i\frac{\hat{T}\tau}{2}\right)\exp(-i\hat{V}\tau)\exp\left(-i\frac{\hat{T}\tau}{2}\right) + o(\tau^3) \tag{7}$$

where $\hat{T}$ and $\hat{V}$ represent the total kinetic and potential parts of the Hamiltonian $\hat{H}$ of (2). The accuracy considerations for the optimal timestep and size of the mesh, along with other details as to how tunnelling probabilities were calculated, can be found elsewhere [24]. In the present case, all quantities were calculated to a numerical accuracy of the order of a few per cent. This requires, typically, propagation of $\sim 10^4$ timesteps on meshes of 2048–4096 and 16–32 points for the electron and oscillator coordinates, respectively. A large number of points is required for the electron because the mesh interval is determined by the barrier width while the extent of the mesh is governed by the required energy resolution, in this case $\sim$ a few tenths of an electron volt. Typically, a mesh spanning $-400 < X < 100$ au was found to give reasonable results for most purposes. A high resolution is necessary not only in order to reproduce structure on the scale of the oscillator frequency, but also to ensure that the part of the wavepacket emerging to the right of the barrier actually went through it and not over it. Very roughly, an electron packet with mean energy ϵ (eV) and confined within region dX (au) has energy resolution $d\epsilon \sim 7\sqrt{\epsilon}/dX$ eV.

Figures 3(*a*)–(*c*) and 3(*d*)–(*f*) illustrate some features of the manner in which the packets propagate for the non-resonant and resonant cases, respectively. Figure 3(*a*) shows the amplitude of a 6.25 eV packet some time after its front edge has struck the non-resonant barrier. The packet amplitude is plotted as a function of electron position, X. A small part of the packet, visible as a weak tail in the region $X > 0$, has penetrated the barrier via tunnelling. The pronounced oscillations over the bulk of the packet for $X < 0$ are due to interference between incoming and reflected waves. Some time later, the packet has the form shown in figure 3(*b*). The transmitted and reflected packets have now all but separated and the main peak is moving in the $-X$ direction towards the left mesh edge. The sharp edge in the transmitted packet towards the right mesh edge is due to the 'absorbing wall' boundary condition employed to absorb the packet [26]. The absence of 'interference ripples' on this part of the packet is an indication that the walls really are 'black'. The tunnelling probability was evaluated by integrating the instantaneous current passing through $X = +50$ au, halfway between the barrier and the absorption region. The behaviour of the current as a function of time is shown in figure 3(*c*). The plots show the currents, S_ν, associated with projections of the wavepacket onto the oscillator eigenstates, labelled by ν. Since higher levels of excitation correspond to slower electrons in the final state, the peaks of the current distributions are displaced slightly in time by an amount roughly proportional to ν. The displacements are very much smaller than the width of the plots, which depend on the real-space width of the initial packet. This is because the oscillator energy of 0.25 eV is small compared with the overall kinetic energy in the final state, 2.25, 2.0, 1.75 eV $\cdots$, so the velocities are too close to allow a marked separation over the relatively short flight path to the point where the current is calculated. The distributions would separate in time if the packet were allowed to propagate far enough but, clearly, there is no point in doing this. Partial probabilities are very much more easily determined via projection of the wavepacket on the oscillator eigenfunctions and determination of the partial currents. These are local quantities and, provided the absorbing walls are sufficiently 'black', are unaffected if the part of the packet that has passed the reference point or plane where the current is calculated is absorbed. The time integrals of the current plots give the probabilities for the electron to tunnel leaving the oscillator in state ν. The packet projections in figures 3(*a*) and (*b*) corresponded to times $t = 300$, 500, respectively, in the wings of the time-of-flight current plot (figure 3(*c*)).

Similar plots in figures 3(*d*)–(*f*) illustrate the build-up and decay of the resonance for the resonant barrier. Figure 3(*d*) shows the packet amplitude at $t = 300$, when the resonance is building up and figure 3(*e*) when it is well in the process of decay ($t = 500$). For this

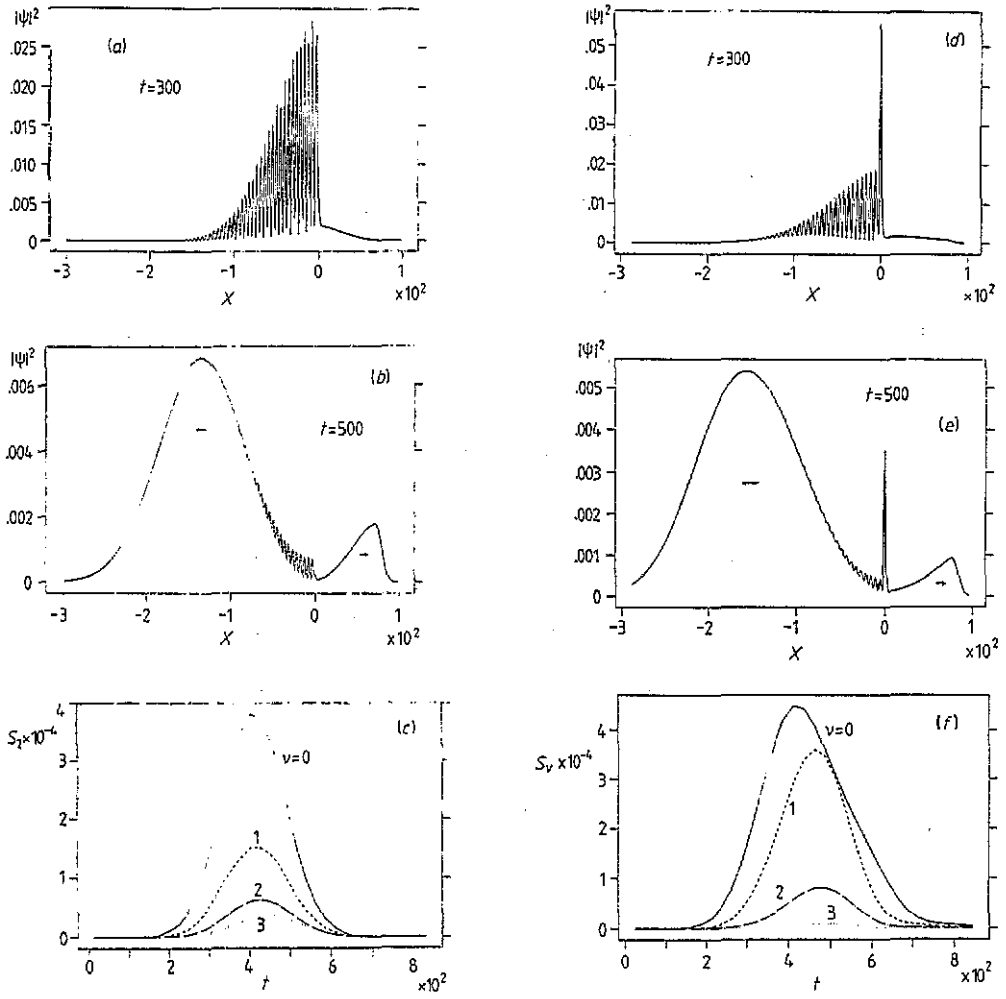

Figure 3. Wavepacket densities and currents for the barriers shown in figures 2(*a*) and (*b*) and incident packet energies of 6.25 and 5.0 eV for the non-resonant (*a*)–(*c*) and resonant (*d*)–(*f*) cases, respectively. (*a*) and (*d*) show wavepacket density distributions as the tunnelling begins ($t = 300$); (*b*) and (*e*) show the corresponding distributions as the tunneled and reflected parts of the packet separate ($t = 500$). (*c*) and (*f*) show partial time-of-flight current distributions through $X = 50$ au, halfway between the tunnelling barrier and the mesh edge, projected onto the final state of the oscillator. The peaks of the partial distributions are displaced in time as the final-state oscillator energy increases, but the displacements are much smaller than the packet widths.

case, with an incident energy of 5.0 eV, the reflected packet carried 80% of the weight (i.e. the total tunnelling probability was about 0.2). The corresponding partial currents are shown in figure 3(*f*)). The oscillator energy is now 1.0 eV so differences in final kinetic energy are larger than for the non-resonant case. However, the net delay of a given packet component is no longer determined by the time of flight alone because the time spent 'in the resonance' is not a single number but depends on the decay mode. This is the reason why the partial current plots in figure 3(*f*) show a somewhat more complex time behaviour than those in figure 3(*c*), for the non-resonant case.

As mentioned above, an important advantage of the wavepacket method is its flexibility.

This is exemplified by the fact that going from the non-resonant barrier to the resonant involves no change in the essential computational effort. In fact, of the two, the resonant case is the easier because the tunnelling probabilities of relevance are of order 10% or greater, whilst those for the non-resonant barrier were typically of order 1%. Clearly, the smaller the number to be calculated, the more care is required to eliminate possible sources of error (e.g. reflection from the mesh edge, timestep errors). Other factors that are of prime importance in achieving analytic results, such as the complexity of the potentials and the couplings, are not material at all in the wavepacket method. Thus, whereas we have used a linear coupling to the oscillator, this is merely so that results can be compared to other calculations where a linear coupling had to be assumed in order to obtain a solution. No extra work is needed at all to deal with couplings of arbitrary strength and complexity.

This advantage of the method is off-set by its main disadvantage, which is resolution. A major point of interest in the non-resonant case is behaviour at thresholds where a tunnelling electron can first excite a vibrational mode. To study threshold behaviour, a resolution is required that is sufficient to reveal singular behaviour as a new channel turns on. In the present case (and probably in general) it turned out to be impractical to run packets having the required resolution. Accordingly, we studied threshold behaviour with the aid of coupled channels calculations using a method analogous to that of Gelfand and co-workers [27]. The scattering wavefunction was expanded in states, ν, of the bare harmonic oscillator. Numerical solutions of the one-dimensional channel Schrödinger equation corresponding to a given ν were then determined by numerical integration using 'left' and 'right' scattering boundary conditions. These were then used as 'left' and 'right' basis sets and the full wavefunction corresponding to a given set of incidence conditions was determined as a matching problem at the centre of the barrier. As usual in such cases, the convergence of the method was not easy to establish internally because of oscillatory behaviour as ν_{max} was increased. In the present case, an absolute check on convergence was available by running the code off-threshold and checking against the packet calculations. This was particularly important for strong coupling, where it was found necessary to include over 400 channels in the calculation.

3. Inelastic non-resonant tunnelling

Figure 4(a) shows $\Delta T(\epsilon, V_c)$, the oscillator-induced change in tunnelling probabilities as a function of initial kinetic energy, ϵ, obtained from wavepacket calculations using the non-resonant barrier depicted in figure 2(a) with an oscillator energy of 1.0 eV. The term $\Delta T(\epsilon, V_c)$ is defined as the difference between the total tunnelling probability, $T_{tot}(\epsilon, V_c)$, with the inelastic coupling switched on and the tunnelling probability $T_0(\epsilon) \equiv T_{tot}(\epsilon, V_c = 0)$ of the bare barrier with the oscillator switched off, i.e. $T_{tot}(\epsilon, V_c) = T_0(\epsilon) + \Delta T(\epsilon, V_c)$. For the barrier shown in figure 2(a) and a moderate coupling strength, T_0 is by far the largest contribution to the tunnelling having the value 0.057 at 6.25 eV incident energy. Coupling to the oscillator contributed an additional tunnelling probability of about 25% of the total at all energies. We display ΔT rather than the total probability in figure 4(a) to highlight the slope discontinuities that occur at the thresholds. The opening of each new channel gives rise to a sudden increase in the slope of the total tunnelling current (the increase is visible only for the $\nu = 1$ threshold at 5 eV). Also shown in figure 4(a) are the partial contributions to ΔT that correspond to tunnelling with the oscillator left in its νth excited state. The partial contributions are identically zero below the corresponding threshold incident kinetic

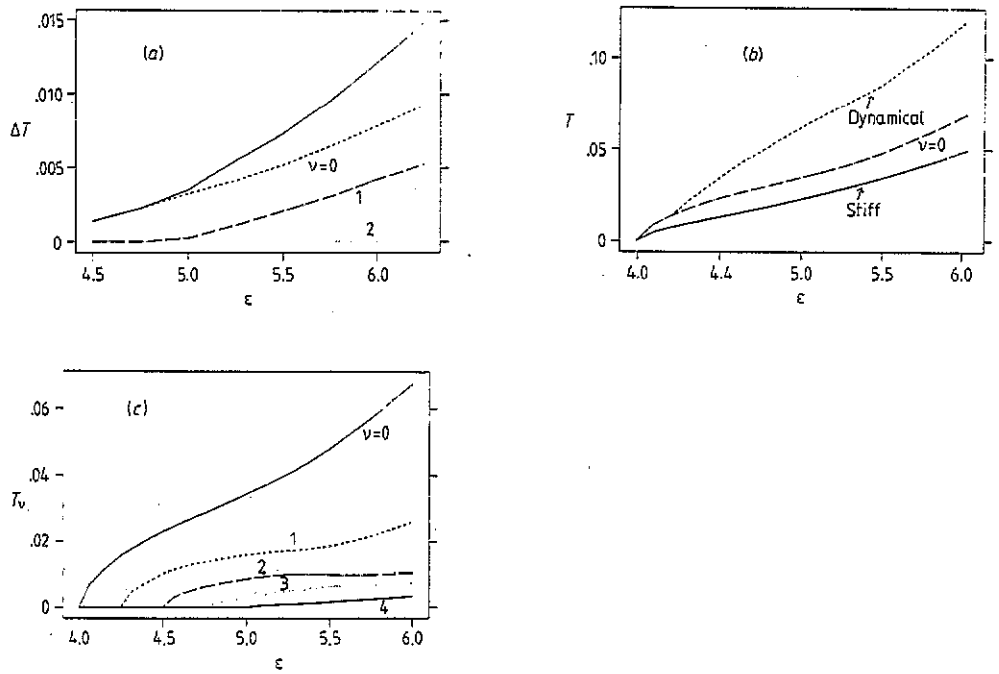

Figure 4. Tunneling characteristics of the non-resonant barrier in figure 2(*a*). (*a*) Oscillator-induced changes in tunnelling probability for barrier with 1 eV oscillator, showing the discontinuous increases in the total (full curve) as new channels open. The broken, chain and dotted curves give the partial probabilities projected onto final oscillator states with $\nu = 0, 1, 2$. The threshold behaviour is given incorrectly because of the finite packet resolution. (*b*) Comparison of the tunnelling characteristic of the non-resonant barrier with the oscillator ($\epsilon_{osc} = .25$ eV) switched on and off. The full curve refers to the characteristic of the bare barrier. The broken curve shows how this increases when the oscillator is switched on. The chain curve gives the elastic component of the dynamical barrier (i.e. projected onto $\nu = 0$). This contribution alone corresponds to a substantial enhancement of the stiff-barrier characteristic. (*c*) Partial tunnelling probabilities with 0.25 eV oscillator illustrating the square-root singularities at the onset of transmitted channels.

energy, $V_R + \nu\epsilon_{osc}$, and it is their onset that is responsible for the discontinuities in slope of $\Delta T(\epsilon)$ (and so the total tunnelling probability).

The behaviour found in the wavepacket calculations and illustrated in figure 4(*a*) is typical of what is found in differential inelastic tunnelling spectroscopy [28]. The onset of a new channel coincides with a discontinuous *increase* in the net tunnelling probability. Clearly, each new channel adds its contribution to the total, but it is not obvious why the increase should not be compensated by a concomitant depletion of other channels. A naive (and incorrect) view of the interaction between the oscillator and the tunnelling electron regards this solely in terms of excitation or not of the oscillator as the particle traverses the barrier. This view can lead to confusion with respect to unitarity, which of course must hold for all channels, but does not hold for any subset of channels, such as the subset of all transmitted channels. If this were the case, then there would be no discontinuous changes in the *total* tunnelling probability at thresholds at all because the contribution of the emerging channel would be cancelled exactly by a depletion of other channels, as occurs for example in helium beam scattering from a surface when the beam energy sweeps through a selective adsorption threshold [29]. A correct view of inelastic tunnelling processes recognizes that

rigid barriers and barriers with internal dynamics are intrinsically different in their behaviour. No problems ensue if the scattering process is viewed as starting in the leads and not in the barrier itself. An electron approaches the junction and will either tunnel through or reflect back into the leads, in either case with or without excitation of the oscillator. Unitarity obtains with respect to all transmitted and reflected channels but does not obtain for either subset alone and, in fact, the onset of a new transmission channel may be associated with a net enhancement, no change, or a net depletion of the total tunnel probability.

To illustrate in detail what actually happens at onset we show in figures 4(*b*) and (*c*) data obtained via coupled channels calculations, as outlined above. These data were calculated for the case $\epsilon_{osc} = 0.25\,\text{eV}$, an oscillator energy more typically relevant for STM, and coupling parameter $V_c \sim 7.5\,\text{eV}$. The number of open channels over the energy range spanning the barrier height, and the overall coupling to the oscillator is now significantly increased. Figure 4(*b*) compares the total and elastic tunnelling probabilities with the tunnelling probability in the absence of coupling. Switching on the oscillator now enhances the tunnel probability greatly, by more than a factor of two for incident energies greater than 5.3 eV. As in figure 4(*a*) for the stiffer oscillator, this enhancement is not at all restricted to the inelastic channels but occurs also for the elastic channel. This is because the polarization of the oscillator acts as an effective attractive interaction assisting the electron's passage through the barrier. The effect leads to a strong increase in the tunnelling current over its value for the stiff barrier even when the incident electron energy is below the lowest threshold for inelastic tunnelling. The behaviour at channel onsets is not easy to see in figure 4(*b*) but is clear in figure 4(*c*), where partial tunnelling probabilities, elastic ($\nu = 0$) plus the four lowest inelastic $\nu = 1$–4 contributions, are shown separately. The behaviour at threshold is now seen to be a square root singularity in the partial probability that is going to zero, with no concomitant structure at all in the other partial transmission probabilities. The origin of the singularities is evident on writing down the unitarity requirement on the transmission and reflection coefficients, $t_\nu(\epsilon), r_\nu(\epsilon)$ that multiply the transmitted and reflected waves in the wavefunction. Defining the incident wavevector $k_i \equiv \sqrt{2m\epsilon}$ and channel wavevectors for reflection and transmission, $k_\nu^r \equiv [2m(\epsilon - \epsilon_\nu)]^{1/2}$, $k_\nu^t \equiv [2m(\epsilon - \epsilon_\nu - V_R)]^{1/2}$, then the overall conservation of electron current requires that

$$\sum_\nu k_\nu^r |r_\nu(\epsilon)|^2 + \sum_\nu k_\nu^t |t_\nu(\epsilon)|^2 = k_i \tag{8}$$

where the ν sums run over all open channels; V_R is the 'bias' voltage on the junction, i.e. the potential energy difference between $\pm\infty$. As ϵ sweeps through $\epsilon_\nu - V_R$, the νth transmitted channel emerges with a weight $T_\nu \equiv (k_\nu^t/k_i)|t_\nu(\epsilon)|^2$ that grows away from threshold like a square-root simply because of the factor k_ν^t multiplying the square of the transmission coefficient. This singular onset must be matched somewhere by a concomitant cusp to preserve the unitarity condition so either $T_{\nu'}$ or $R_{\nu'} \equiv (k_{\nu'}^r/k_i)|r_{\nu'}(\epsilon)|^2$, with $\nu' \neq \nu$, or R_ν must display a downward cusp as the νth transmission channel opens. For the potential that generated the data in figure 4, the downward cusp is clearly not present in $T_{\nu'}$ and is in fact in the reflected channel R_ν. That is, the main singularities occur within the same subspace, ν, and refer to matching singular onset and concomitant cusp in T_ν and R_ν, respectively, as illustrated in figure 5(*a*). Other channels do display irregularities at the threshold but these are of lesser importance. The reason why the total tunnelling probability increases as each channel opens in figure 4(*b*) is simply that the transmitted channel opens with a singular onset and the concomitant singular depletion occurs in a reflected channel. The total tunnelling then profits from practically all of the current flowing in the new channel.

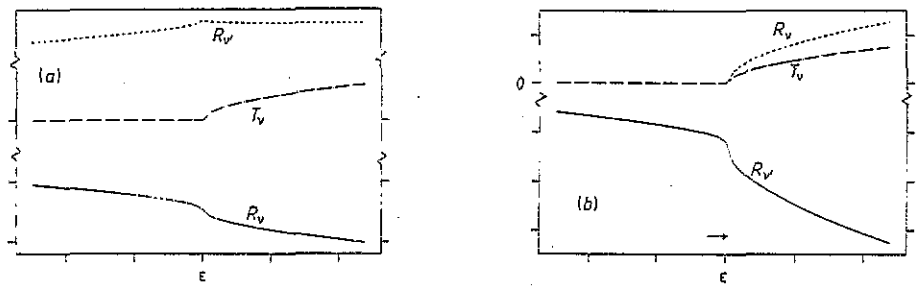

Figure 5. Typical threshold behaviour for non-resonant tunnelling. (*a*) Asymmetric barrier. Here the onset singularity of the νth transmitted channel is accompanied by a companion singular cusp in the νth reflected channel. (*b*) Symmetric barrier. The νth transmitted and reflected channels onset at the same energy. The companion cusp then occurs in a $\nu' \neq \nu$ channel or channels, depending on details. The case shown is particularly simple and the companion cusp occurs in a single channel, $\nu = 0$ reflection.

We speculate that this behaviour will be observed generally provided the channels emerge one at a time with no coincidences or interferences.

Gelfand and co-workers [27] considered the case of zero bias, $V_R = 0$, where the singular behaviour is more complex because $k_\nu^r(\epsilon) = k_\nu^t(\epsilon)$ and the νth reflected and transmitted channels emerge at exactly the same energy. Since both channels then display singular onsets, the concomitant cusps required for unitarity must occur in some other subspace, $\nu' \neq \nu$. This is illustrated in figure 5(*b*), where the threshold behaviour observed using a symmetric potential is sketched. In the particular case shown the main channel that is depleted is the elastic reflection channel, R_0, and in fact the total tunnel current decreases as the energy sweeps through threshold. The precise behaviour, however, depends on details of potential and coupling. In general, as Gelfand and co-workers found, the concomitant cusp is shared by several other channels and the set of onset singularities may result in an increase or depletion of the total tunnelling probability. This situation we believe will result in general only when the coupling is extremely strong and/or when energetically coincident or strongly interfering thresholds for transmission and reflection occur.

We have noted that the interaction of the electron with the oscillator cannot be thought of as independent from the tunnelling process as a whole. The forced-oscillator model implies a de-coupling of tunnelling and inelasticity, with the latter treated by assuming the particle traversing the tunnelling barrier gives rise to a time-dependent force on the oscillator that switches on and off, and so cannot be right in detail. It is nevertheless legitimate to ask whether the model reproduces the *relative* probabilities, P_ν, with which the oscillator is left in excited state ν. As noted in the introduction, within the forced-oscillator model the P_ν form a Poisson distribution characterized by a single parameter β which measures essentially the time average of the coupling strength. An analysis of the relative probabilities in figure 4(*c*) showed that these fall off significantly more slowly than Poisson. This is a typical consequence of a 'slow' interaction, where the dynamics of the 'target' (i.e. the oscillator) works back onto the trajectory of the 'projectile' and the overall motion takes on some elements of adiabaticity. Since the parameters used to generate the tunnelling data in figure 4 are typical for applications in STM, this conclusion as to the validity of a semiclassical description probably holds in this context.

4. Inelastic resonant tunnelling

The qualitative behaviour of the resonant tunnelling barrier in figure 2(*b*) as given by the wavepacket calculations is illustrated in figures 6(*a*) and (*b*). Figure 6(*a*) shows the effect of increasing the coupling gradually. The curve marked 'Wave' is for the stiff-barrier alone and was determined using a wavematching method. This gives the true infinite-resolution tunnelling characteristic of the barrier, which becomes transparent at the peak of the resonance at an energy of $\epsilon_{res} = 4.92\,\text{eV}$. Basically, the stiff-barrier characteristic is a single peak with full width at half-maximum $\sim 0.3\,\text{eV}$ superposed on a low, weakly varying background. A wavepacket that would reproduce this behaviour quantitatively must have a resolution significantly less than the width, which would require an initial packet spread in X of many hundred au. This can be done, but requires undesirably long propagation times. We compromised by using an initial packet having an estimated energy resolution of approximately the resonance width. This gave the stiff-barrier characteristic marked 'Packet'. The main consequences of the finite energy spread are a peaking of the tunnel probability at ~ 0.6 rather than unity and a somewhat broadened resonance structure. This was regarded as sufficiently similar to the correct result to allow a sensible study of inelastic effects.

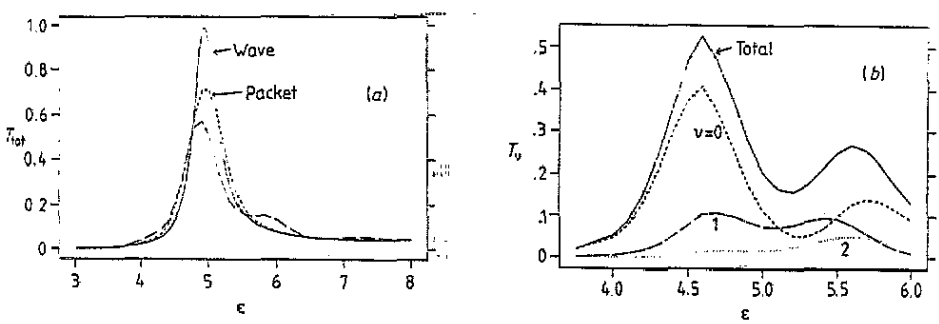

Figure 6. Tunneling through barrier with resonance state. (*a*) Total elastic transmission through rigid barrier as determined by a wavematching method (full curve). The broken curve gives the equivalent using a packet with a resolution of approximately the resonance width. The chain and dotted curves give the effect of a weak and stronger coupling to oscillator ($\epsilon_{osc} = 1\,\text{eV}$). (*b*) The full, broken, chain and dotted curves give the total, elastic and first two inelastic channel transmission characteristics as function of incident particle energy and for the case of stronger coupling.

When the oscillator coupling is switched on the broken curve goes over in sequence into the chain curve and the dotted curve as the coupling strengthens. In the non-resonant case, the coupling enhanced the tunnelling at all energies and inelastic effects were qualitatively (though not quantitatively) in accord with a semiclassical picture of the trajectorized electron–displaced-oscillator interaction. The same is not true when resonances are present, however, because even a nominally weak coupling is enhanced hugely by the resonant time delay of the electron within the barrier. The semiclassical picture discussed above for the non-resonant case then fails and the tunnelling behaviour cannot at all be deduced in terms of a perturbation on stiff-barrier behaviour. If the oscillator energy is larger than the natural width of the stiff-barrier resonance, the coupling splits this resonance into a family of resonances separated by roughly the oscillator energy, as in figure 6(*a*), for which $\epsilon_{osc} = 1.0\,\text{eV}$. The lowest member of the family is shifted down in energy with

respect to ϵ_{res} by an amount $\delta\epsilon_{res} = \lambda_0^2/\epsilon_{osc}$ that depends on the square of the coupling. The effect is analogous to the overall enhancement of the elastic tunnelling for a non-resonant barrier but now involves the temporary formation within the barrier of a 'quasi-polaron' (in fact, for sufficiently strong coupling the resonance would shift to negative energy and become a genuine polaron). The higher-lying resonances can also be thought of in terms of quasi-polarons that can be labelled according to the excitation spectrum of the bare oscillator. However, this does not mean that the decay of the νth quasi-polaron leaves the oscillator in its νth excited state. Figure 6(b) shows partial tunnelling probabilities, $T_\nu(\epsilon)$, giving the transmission characteristic when the oscillator is left in state $\nu = 0, 1, 2$. The interpretation of these characteristics will be considered presently.

It is interesting to compare the data in figure 6 with equivalent results obtained via the analytic method of Wingreen and co-workers [13], who studied the more simplified but physically related model specified by (1) using a Green function method. They showed that the total transmission probability through a resonant barrier for an incident electron with energy ϵ is given by

$$T_{tot}(\epsilon) = \sum_{\nu=0}^{\infty} T_\nu(\epsilon) \tag{9}$$

where the partial transmission function for electron tunnelling accompanied by excitation of ν vibrational quanta ($\nu = 0$ is the elastic channel) is

$$T_\nu(\epsilon) = \Gamma_l\Gamma_r \frac{\beta^\nu}{\nu!} e^{-2\beta} \left| \sum_{m=0}^{\infty} \sum_{j=0}^{\nu} \frac{B_{\nu,m,j}}{\epsilon - (\epsilon_a - \delta\epsilon_{res}) - (m+j)\epsilon_{osc} + i\Gamma/2} \right|^2 \tag{10}$$

with $B_{\nu,m,j} \equiv (-1)^j \binom{\nu}{j} \frac{\beta^m}{m!}$. As mentioned in section 1, the electron–oscillator coupling strength is characterized by the ubiquitous parameter $\beta = \{\lambda_0/\epsilon_{osc}\}^2$ which most obviously enters as an overall negative shift, $\delta\epsilon_{res} \equiv \beta\epsilon_{osc}$, to the unperturbed spectrum. The total width of the resonance in (10), Γ, is given by the sum of the partial widths, Γ_l, Γ_r, characterizing the decay of the resonance into states of the left or right electrode.

To make contact with the wavepacket calculations in figure 6, we have evaluated (9) and (10) for a symmetric barrier, $\Gamma_l = \Gamma_r = \Gamma/2$, and with parameters $\epsilon_a = 4.92\,\text{eV}$, $\epsilon_{osc} = 1\,\text{eV}$ and constant energy-independent width $\Gamma = 0.6\,\text{eV}$. The evolution of the transmission function as the coupling increases is illustrated in figure 7(a) for the three cases $\beta = 0.0, 0.5, 1.0$. The similarity to the wavepacket results in figure 6(a) is unmistakable. More striking still is a comparison of partial transmission functions. On using a value of $\beta = 0.3$, chosen so that the coupling strength as exemplified by the shift of the resonance energy is the same as for the wavepacket calculations, (10) gave the partial transmission functions shown in figure 7(b). Aside from the straightforward reduction in peak maximum due to the finite energy spread in the wavepackets, the partial spectra in figures 6(b) and 7(b) are to all intents and purposes identical. Within the parameter range investigated here, therefore, the analytic result in (10), obtained on the basis of the displaced oscillator model, provides a highly accurate picture of the inelastic tunnelling. Provided the non-resonant background is fairly flat, $T_{tot}(\epsilon)$ in (9) obeys the simple sum-rules that the zeroth and first energy moments are independent of the electron–oscillator coupling strength [13]. The same sum-rules are also found to be obeyed within the numerical accuracy by the transmission probabilities given by the wavepacket calculations.

The physical content of these sum-rules and the overall behaviour of the tunnel characteristic becomes particularly clear within a two-level treatment of the resonant state,

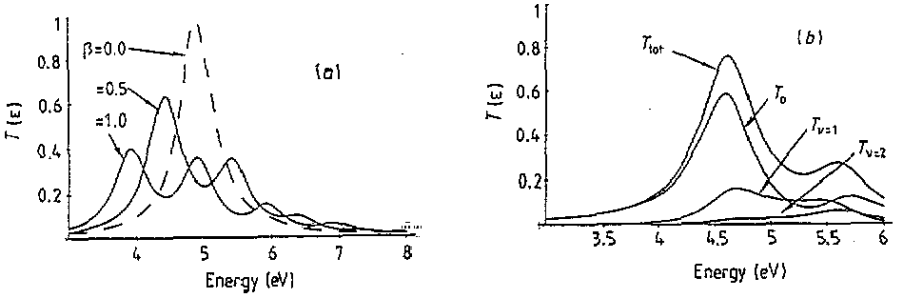

Figure 7. Transmission functions according to (9) and (10). (*a*) Total tunnelling probability, T_{tot}, for three values of coupling strength. (*b*) Partial transmission characteristic, T_v, for a coupling equivalent to that in figure 6(*b*).

where the oscillator is allowed to be in its ground state or first excited state but not in states of higher energy. Ordinarily, the spacing of electronic levels within the resonant well will be much larger than the oscillator energy. The resonant wavefunctions can then be assumed to involve essentially only a single electronic function and so will have the form

$$\Psi(X, Y) = \frac{1}{\sqrt{1+b^2}}\psi_{res}(X)[\chi_0(Y) + b\chi_1(Y)] \tag{11}$$

where $\psi_{res}(X)$ is the resonant state in the absence of coupling (which can be defined precisely by switching off also the coupling to the left and right continua), and $\chi_{0,1}$ are harmonic oscillator eigenfunctions. In the absence of electron–oscillator coupling $\psi_{res}(X)$ is the relevant quasi-bound-state, with energy ϵ_{res}, and the tunnelling characteristic will be a single peak, which, making the usual assumption of a flat background and negligible level shift, will have the Breit–Wigner form

$$T_0(\epsilon) = \frac{\Gamma_i\Gamma_r}{(\epsilon - \epsilon_{res})^2 + \frac{1}{4}\Gamma^2} \tag{12}$$

where Γ_i is the width of the resonance due to decay by the incident channel. For the case of a stiff barrier with zero coupling to the oscillator we have $\Gamma_i = \Gamma_l$ and since the potential is symmetric, $\Gamma_i = \Gamma_r = \Gamma/2$, so the barrier becomes perfectly transparent at the resonance maximum.

If the oscillator is now coupled in via matrix elements

$$V \equiv \langle\psi_{res}|\langle\chi_0|V_c(X, Y)|\chi_1\rangle|\psi_{res}\rangle \tag{13}$$

the single resonant state splits into a doublet whose components can be determined by diagonalizing the Hamiltonian in the 2×2 subspace of oscillator functions. The resonant energies, $\epsilon_\pm$, and the wavefunction parameters $b_\pm$ that appear in (11) are

$$\tilde{\epsilon}_\pm \equiv \epsilon_\pm - \epsilon_{res} = \tfrac{1}{2}[\epsilon_{osc} \pm (\epsilon_{osc}^2 + 4V^2)^{1/2}] \qquad b_\pm = \tilde{\epsilon}_\pm/V \tag{14}$$

and refer to the new quasi-bound states of the full Hamiltonian. These give rise to two distinct resonant structures provided the resonance widths are significantly smaller than the spacing $\epsilon_+ - \epsilon_- \sim \epsilon_{osc}$. As figure 6(*a*) shows, the sub-resonance structures are not carbon copies of the original $V = 0$ structure but have unequal peak heights that are substantially smaller than the $V = 0$ peak height. The reason for this may not at first sight be obvious.

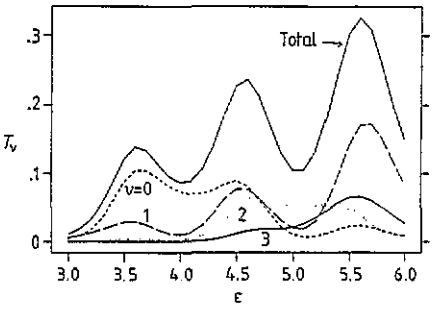

Figure 8. Wavepacket calculation of the transmission function for a 'hot' junction in which the oscillator is initially in the first excited state. This illustrates the effect of *assisted tunnelling* where the oscillator de-excites during the tunnelling process. Total and partial transmission functions into first four channels are shown.

If the matrix elements that determine the partial widths, Γ_l, Γ_r, have only a weak energy dependence across the spectrum of energies, then these widths are essentially *independent* of the value of V. The resonance can decay into states of the left or right continuum leaving the oscillator either in its ground state, or singly excited. The coupling strength influences these partial probabilities but normalization within the oscillator subspace ensures that the overall decay probabilities, determined by the overlap of ψ_{res} with left or right band functions, are unaffected.

The same is not true of the *incident* width Γ_i, however, because this corresponds to the oscillator being in its ground state. Thus, the resonance width due to decay via the incident channel includes an additional reduction factor expressing the weight of the oscillator ground state in the resonant state, namely

$$\Gamma_i^{\pm} = R_{\pm}\Gamma_l \qquad R_{\pm} \equiv \frac{V^2}{V^2 + \tilde{\epsilon}_{\pm}^2}. \tag{15}$$

Accordingly, the maximum values of the sub-peaks due to the individual sub-states of the resonant doublet are reduced from unity to $R_{\pm}$, and the weights of the substructures are decreased correspondingly. As can easily be verified explicitly for the two-level example, the reduction factors and resonance energies obey

$$R_+ + R_- = 1 \qquad R_+\epsilon_+ + R_-\epsilon_- = \epsilon_{res} \tag{16}$$

results that follow from the fact that the level wavefunctions for different V are related via a unitary transformation within the subspace of oscillator levels. Clearly, (16) can be trivially generalized to N levels and reveals the physical origin of the sum-rules derived by Wingreen and co-workers, and referred to above. These state that the zeroth and first energy moments of the tunnel characteristic are independent of the electron–oscillator coupling. The sum-rules assume the energy dependence of all relevant decay matrix elements is weak, but more importantly, that the resonant state is dominated by a single quasi-bound electronic level, as in (11). If the electronic–vibronic coupling draws higher-lying electronic levels into the quasi-bound-states, the widths due to decay into the left and right electrodes would depend strongly on the coupling. Use of (1) rules this out explicitly, so the single-state assumption is implicit in the work of Wingreen and co-workers. There is no such stipulation in the model Hamiltonian (2) used in the wavepacket calculations, but the fact that the results agree with the analytic formula and the sum-rules are obeyed approximately is *a posteriori* evidence that the condition holds approximately nevertheless. This discussion shows that the model Hamiltonian in (1) gives an excellent description of inelastic resonance tunnelling provided the separation of the electronic levels is much larger than the vibrational quanta responsible for the inelasticity.

Finally, figure 8 shows the result of a calculation where the oscillator is initially in its first excited state so that assisted tunnelling is possible, with the electron gaining energy and the oscillator reverting to its ground state. In non-resonant tunnelling this leads to an exponential increase of the total probability because the absorption of the initial oscillator energy propels the incident particle towards the top of the tunnelling barrier [30]. In resonant tunnelling, the effect is different. Gain processes give rise to a new resonance in the total tunnelling probability, $T^1(\epsilon)$, which now displays three resonances in the energy range considered. They are displaced downwards by about ϵ_{osc} compared with the structures in figure 6 because the energy scale refers to the kinetic energy of the incident particle, which is smaller than the initial total energy by the oscillator energy, ϵ_{osc}. Otherwise, the behaviour is similar. The partial probabilities, $T_\nu^1(\epsilon)$, refer to tunnelling with the oscillator in the final state ν. These follow the breakdown of oscillator eigenstates in the quasi-bound wavefunctions. For example, the highest-lying peak corresponds to a quasi-bound state whose wavefunction contains the largest admixture of χ_1. This is the reason it decays preferentially into the $\nu = 1$ channel. Likewise, the peak heights in the total tunnel probability increase in proportion to the overlap of the corresponding quasi-bound state with the $\nu = 1$ incident state, in qualitative accord with (12) (i.e. Γ_i is largest for the quasi-bound-state having the largest $\nu = 1$ weight). In practice, gain processes will contribute a temperature-dependent broadening, either of the sub-structure in the tunnel characteristic, or of the entire structure if the individual lines are not resolved. Such effects can be estimated from calculations such as those in figures 6 and 8 by thermally weighting contributions with the oscillator initially in different quantum states.

5. Summary and conclusions

The problem of inelastic tunnelling, whether resonant or non-resonant, is of considerable interest both with respect to understanding the physics underlying the performance of devices such as scanning tunnelling microscopes and to development of a useful vibrational spectroscopy. The problem has been considered in many theoretical papers, most of which have employed a number of approximations and simplifications. The central aim of this paper has been to revisit and shed new light on some of the issues with the aid of numerically exact wavepacket calculations. Specifically, we have used wavepackets to model the tunnelling of a hot electron that has, for example, been photoexcited to a conduction band by an ultra-fast laser pulse, through a junction where dynamical coupling to a vibrational mode, modelled as a harmonic oscillator, occurs. Both non-resonant and resonant coupling has been considered. In the non-resonant case, the focus of the calculations was on threshold behaviour and the derivative discontinuities in the total tunnelling current that occur when the energy (gate voltage) sweeps through a vibrational onset. We found that the overall tunnelling current increases each time a new channel opens, as commonly found in experimental differential inelastic tunnelling spectroscopy. We showed that this was due to the manner in which the singular onset of a new channel is matched with concomitant cusp singularities that maintain unitarity. If the νth reflection channel is already open when the νth transmission channel opens then this provides the concomitant cusp. Accordingly, the total tunnel current increases as the energy sweeps through threshold. We expect this to hold in general for not too large coupling unless the νth reflection and transmission channels open at the wave same energy (symmetric potential). In this case, treated by Gelfand and co-workers [27], the concomitant cusp is taken up by channels with $\nu' \neq \nu$. These could be predominantly reflection or transmission channels and the total tunnelling current may increase or decrease through threshold, depending on details.

In treating resonant scattering, our main concerns were to demonstrate how the wavepacket method can be applied to the resonant electron tunnelling problem and to establish contact with analytic theory based on simplified models. We found that the inelastic coupling to the vibrational mode gives rise to a sub-structure in the tunnelling characteristic that, for the specific choice of potential and coupling used in the calculation, was reproduced almost perfectly by the analytic formula derived by Wingreen and co-workers [13] on the basis of the model Hamiltonian (1). The reason for this was discussed in detail in terms of a two-level Breit–Wigner model, which allowed a pleasing physical interpretation of the resonant inelastic tunnelling process and established a physical basis for the simple sum-rules obeyed by the analytic tunnelling formulae [13]. The analysis also makes clear that the analytic formula and the sum-rules will fail if the oscillator couples strongly to two or more electronic levels, or involves the continuum of electronic levels in an essential way. In the wavepacket calculations, no assumptions were made explicitly on this point, and the method is no harder to implement when an arbitrary number of levels rather than only a single level is involved. However, the good agreement with the analytic formula shows that for the potentials and coupling parameters chosen, basically only a single electronic resonant level contributed.

Acknowledgments

We gratefully acknowledge a grant of CPU time by the HLRZ, Forschungszentrum Jülich and assistance from Mark Stiles at NIST.

References

[1] Kelly M J and Nicholas R J 1985 *Rep. Prog. Phys.* **48** 1699
Reed M A and Kirk W P (eds) 1989 *Nanostructure Physics and Fabrication* (New York: Academic)
Chamberlain J M, Eaves L and Portal J C (eds) 1990 *Electronic Properties of Multilayers and Low-Dimensional Semiconductor Structures* (New York: Plenum)
Davies J H and Lang A R (eds) 1992 *Physics of Nanostructures* (Bristol: IOPP)

[2] Burstein E, Lundqvist S and Tosatti E 1988 *Phys. Scri.* **38** 233–320
Behm R J, Garcia N and Rohrer H (eds) 1990 *Scanning Tunneling Microscopy and Related Methods* (Dordrecht: Kluwer)

[3] Duke C B and Alferieff M E 1967 *J. Chem. Phys.* **46** 923
Plummer E W, Gadzuk J W and Young R D 1969 *Solid State Commun.* **7** 487
Gadzuk J W and Plummer E W 1973 *Rev. Mod. Phys.* **45** 487
Penn D R, Gomer R and Cohen M H 1972 *Phys. Rev.* B **5** 768

[4] Tersoff J and Hamann D R 1985 *Phys. Rev.* B **31** 805
Lang N D 1987 *Phys. Rev.* B **36** 8173
Lang N D, Yacoby A and Imry Y 1989 *Phys. Rev. Lett.* **63** 1499
Gadzuk J W 1993 *Phys. Rev.* B (submitted)

[5] Persson B N J and Baratoff A 1987 *Phys. Rev. Lett.* **59** 339
Persson B N J 1988 *Phys. Scri.* **38** 282

[6] Himpsel F J 1991 *Phys. Rev.* B **44** 5966

[7] Hauge E H and Stovneng J A 1989 *Rev. Mod. Phys.* **61** 917
Huang Z H, Cutler P H, Feuchtwang T E, Kazes E, Nguyen H Q and Sullivan T E 1990 *J. Vac. Sci. Technol.* A **8** 186 (1990)
Jonson M E 1990 *Quantum Transport in Semiconductors* ed. D Ferry and C Jacobini (New York: Plenum)

[8] Büttiker M and Landauer R 1982 *Phys. Rev. Lett.* **49** 1739

[9] Büttiker M 1989 *Nanostructure Physics and Fabrication* ed. M A Reed and W P Kirk (New York: Academic)
Landauer R 1991 *Ber. Bunsenges. Phys. Chem.* **95** 404

[10] Jauho A P and Jonson M 1989 *J. Phys.: Condens. Matter* **1** 9027

[11] Jauho J P 1990 *Phys. Rev.* B **41** 12327
Johansson P 1990 *Phys. Rev.* B **41** 9892
Wingreen N S 1990 *Appl. Phys. Lett.* B **56** 253
[12] Glazman L I and Shekter R I 1988 *Solid State Commun.* **66** 65; 1988 *Sov. Phys.–JETP* **67** 163
[13] Wingreen N S, Jacobsen J W and Wilkins J W 1989 *Phys. Rev.* B **40** 11834
[14] Jonson M 1989 *Phys. Rev.* B **39** 5924
Lopez-Castillo J M, Tannous C and Jay-Gerin J P 1990 *Phys. Rev.* A **41** 2273
[15] Almbladh C O and Minnhagen P 1978 *Phys. Rev.* B **17** 929
Mahan G D 1981 *Many-Particle Physics* (New York: Plenum)
Cini M and D'Andrea A 1988 *J. Phys. C: Solid State Phys.* **21** 193
[16] Langreth D C, Müller-Hartman E, Ramakrishnan T V and Toulouse G 1971 *Phys. Rev.* B **3** 1102
Mayan G D 1974 *Solid State Physics* **29** ed. H Ehrenreich, D Turnbull and F Seitz (New York: Academic) p 75
Citrin P H, Wertheim G K and Schlüter M 1979 *Phys. Rev.* B **20** 3067
Sunjić M 1980 *Phys. Scri.* **21** 561
von Barth U and Grossmann G 1982 *Phys. Rev.* B **25** 5150
Gumhalter B 1984 *Prog. Surf. Sci.* **15** 1
Gunnarsson O and Schönhammer K 1984 *Many-Body Phenomena at Surfaces* ed. D Langreth and H Suhl (New York: Academic) p 221
Cini M and D'Andrea A 1984 *Phys. Rev.* B **29** 6540
Cederbaum L S and Domcke C 1977 *Adv. Chem. Phys.* **36** 205
Gadzuk J W 1979 *Phys. Rev.* B **20** 515
Cini M 1984 *Phys. Rev.* B **29** 547
Domcke W and Cederbaum L S 1977 *J. Phys. B: At. Mol. Phys.* **10** L47; 1980 *J. Phys. B: At. Mol. Phys.* **13** 2829
[17] Gadzuk J W 1991 *Phys. Rev.* B **44** 13466
[18] Kerner E H 1958 *Can. J. Phys.* **36** 371
Rapp D 1971 *Quantum Mechanics* (New York: Holt, Rhinehardt and Winston) pp 435–72
[19] Tannor D J and Rice S A 1988 *Adv. Chem. Phys.* **70** 441
Hirschfelder J O 1989 *Adv. Chem. Phys.* **73** 1
Brumer P and Shapiro M 1992 *Ann. Rev. Phys. Chem.* **43** 257
Porter E D, Herck J L, Pedersen S, Liu Q and Zewail A H 1992 *Nature* **355** 66
Cavanagh R R, King D S, Stephenson J C and Heinz T F 1993 *J. Phys. Chem.* **97** 786
[20] Coalson R D 1987 *J. Chem. Phys.* **86** 995; 1989 *Adv. Chem. Phys.* **73** 605
[21] Gadzuk J W 1988 *Ann. Rev. Phys. Chem* **39** 395
[22] Brandt S and Dahmen H D 1985 *The Picture Book of Quantum Mechanics* (New York: Wiley)
[23] Feit M D, Fleck J A and Steiger A 1982 *J. Comp. Phys.* **47** 412
Kosloff D and Kosloff R 1983 *J. Comp. Phys.* **52** 35
Kosloff R 1988 *J. Phys. Chem.* **92** 2087
Mohan V and Sathyamurthy N 1988 *Comp. Phys. Rep.* **7** 213
Kulander K C (ed) 1991 *Time-dependent Methods for Quantum Dynamics (Comp. Phys. Commun.)* **63**
[24] Bringer A and Harris J 1989 *J. Chem. Phys.* **91** 7693
[25] Bringer A and Harris J 1992 *Surf. Sci.* **274** 403
[26] Cerjan C and Kosloff R 1986 *Phys. Rev.* B **34** 3832
[27] Gelfand B Y, Schmidt-Rink S and Levi A F J 1989 *Phys. Rev. Lett.* **62** 1683
[28] Wolfram T (ed) 1978 *Inelastic Electron Tunneling Spectroscopy* (Berlin: Springer)
Hansma P K (ed) 1982 *Tunneling Spectroscopy: Capabilities, Applications and New Technologies* (New York: Plenum)
[29] Celli V 1984 *Many-Body Phenomena at Surfaces* ed. D Langreth and H Suhl (New York: Academic) p 315
[30] Harris J, Simon J, Luntz A C, Mullins C B and Rettner C T 1991 *Phys. Rev. Lett.* **67** 652